Multiple-Scales Solution to the Acoustic Boundary Layer in Solid Rocket Motors

J. Majdalani* and W. K. Van Moorhem†

University of Utah, Salt Lake City, Utah 84112

The acoustic boundary-layer structure is investigated in a cylindrical tube where steady sidewall injection is imposed upon an oscillatory flow. Culick's steady, rotational, and inviscid solution is assumed for the mean flow. The time-dependent velocity is obtained by superimposing the acoustic (compressible, inviscid, irrotational) and the vortical (incompressible, viscous, rotational) velocity vectors. A multiple-scales perturbation technique that utilizes proper scaling coordinates is applied to the axial momentum equation by retaining the viscous terms and ignoring the axial convection of vorticity. A closed-form expression for the time-dependent axial velocity is derived that agrees well with the corresponding numerical solution, cold-flow experimental data, and Flandro's near-wall analytic expression. A similarity parameter that controls the thickness of the rotational region is identified. The role of the Strouhal number in controlling the wavelength of rotational waves is established. An accurate assessment of the amplitude and phase relation between unsteady velocity and pressure components is obtained. Increasing viscosity is found to reduce the depth of penetration of the rotational region.

Nomenclature

a_0 = mean chamber speed of sound, m/s
f = oscillation mode frequency, Hz
k = dimensionless wave number or frequency, $\omega R/a_0$
L = internal tube length
M_b = blowing Mach number, V_b/a_0
P_0 = mean chamber pressure
p = dimensionless pressure, $p*/P_0$
R = effective radius, volume/half of porous area, m
Re = Reynolds number based on sound speed, a_0R/ν
Re_a = acoustic Reynolds number, $k/\delta^2 = \omega R^2/\nu = R^2/\delta_s^2$
r = dimensionless radial position, $r*/R$
r_1 = radial scale, magnified or compressed
S_p = penetration number, $M_b^3 k^{-2}\delta^{-2} = V_b^3\omega^{-2}\nu^{-1}R^{-1}$
St = Strouhal number, $k/M_b = \omega R/V_b$
t = dimensionless time, $t*a_0/R = \tilde{t}/k$
U = Culick's steady flow velocity vector, (U_r, U_z)
U_r = Culick's steady radial velocity, $-r^{-1}\sin\theta$
u = dimensionless velocity, $u*/a_0$
u_z' = acoustic velocity, $\sin(kz)\exp(ikt)$
V_b = injection velocity at the porous boundary, m/s
Y = penetration control parameter, $S_p \ell n(100)$
y = radial distance from the porous wall, $(1 - r)$
y_p = penetration depth, $(1 - r_p)$
z = dimensionless axial position, $z*/R$
β = unsteady velocity-to-pressure phase angle
γ = mean ratio of specific heats
δ_s = Stokes layer thickness, $\sqrt{\nu/\omega}$
δ^2 = inverse of Reynolds number, $\nu/(a_0R)$
ε = inverse of acoustic Reynolds number, $\nu/(\omega R^2)$
θ = $\pi r^2/2$
λ = inverse of the Strouhal number, $1/St$

ν = kinematic viscosity, m²/s
ω = dimensional angular speed in rad/s, $2\pi f$

Subscripts
b = condition at the transpiring boundary
0, 1 = order of perturbation terms

Superscripts
* = dimensional quantity
~ = rotational time-dependent part
' = acoustic time-dependent part

Introduction

THE structure of the laminar, time-dependent boundary layer associated with an oscillating velocity flowfield in cylindrical chambers including steady sidewall injection plays an important role in combustion stability assessments in solid rocket motors.[1-3] Recent numerical solutions,[4-8] cold-flow experiments,[9,10] and theoretical analyses[11,16] have contributed to the general understanding of the boundary-layer character, which is a constant companion of the velocity field. Traditionally, in combustion stability predictions, the oscillatory velocity is assumed to be irrotational and inviscid with an associated quasisteady boundary layer that is confined to a thin viscous region near the transpiring surface. Computational predictions of the velocity field by Roach et al.,[4] and Vuillot and Avalon,[5] and Vuillot,[6] and cold-flow tests by Brown et al.,[10] have shown that the rotational region in such flows, sometimes referred to as the acoustic boundary layer, is actually distributed over a significant portion of the chamber radius. Recent analytical and numerical predictions of the transient evolution of the velocity field prescribed by harmonic endwall[11] and sidewall[12] disturbances have also indicated the important role played by the rotational component of the time-dependent velocity. Flandro,[13-16] using analytical means, attempted several approaches to solve this problem. His first approach used viscosity to explain the damping of shear waves generated at the porous surface.[13,14] To attain a solution, the axial convection of vorticity had to be sacrificed in the momentum equation. The radial convection of vorticity also had to be approximated. In his second approach, the axial convection of vorticity was included while viscous terms were neglected.[15] In his third approach, all of the important terms in the momentum equation

were included to attain a solution using regular perturbations.[16] Since analytical approaches are always attractive in their ability to provide a deeper level of understanding and a detailed physical interpretation of the phenomena at hand, one of the goals of this article is to establish a simple analytic expression for the time-dependent velocity and to clarify the dependence of the oscillatory boundary-layer structure on the various control parameters. Another goal will be to show that a multiple-scales perturbation approach can be successful in treating the resulting momentum equation governing the oscillatory flowfield. A viscous and rotational model requiring satisfaction of the no-slip boundary condition at the sidewall and the symmetry condition at the centerline will be adopted here, reminiscent of the earlier approach used by Flandro.[13,14] A multiple-scales perturbation technique that uses the proper variable transformations will be applied to the unsteady, viscous, rotational momentum equation to extract a closed-form expression for the unsteady velocity. This multiple-scales solution will be found to be in fair agreement with recent experimental data by Shaeffer and Brown,[10] Flandro's near-wall solution,[14] and, to a certain extent, with the more recent results by Flandro.[15,16] It predicts a maximum velocity overshoot of twice the acoustic wave amplitude in the vicinity of the wall (otherwise known as the Richardson effect,[17] which is a characteristic of oscillating flows), and it yields an exact expression for the phase angle between velocity and pressure at the wall. Another ascertainment is that of a single similarity parameter, which we have termed the penetration number, which controls the depth of the rotational region. In addition to the added knowledge that this number furnishes, it allows significant simplifications to be made in the expressions for existing models. While the penetration number controls the shape and size of the outer boundary-layer envelope, the Strouhal number will be found to be the agent in control of the rotational wavelength in the radial direction.

Analysis

Following the usual assumptions used in unsteady internal flowfield modeling and combustion instability,[1] the total velocity is separated into two parts, $u = M_bU + u^{(1)}$: 1) a steady, mean flow component (M_bU) that is well modeled by the Culick profile,[18] and 2) an unsteady velocity field that is small in amplitude by comparison to the steady Culick profile.[18] It is this unsteady velocity field that we propose to investigate here.

Fundamental Equations

The first-order unsteady motion is governed by the viscous momentum balance equation[13,15]:

$$\frac{\partial u^{(1)}}{\partial t} + M_b\{\nabla[u^{(1)} \cdot U] - u^{(1)} \times (\nabla \times U) - U \times [\nabla \times u^{(1)}]\}$$

$$= \delta^2 \left\{\frac{4}{3}\nabla[\nabla \cdot u^{(1)}] - \nabla \times [\nabla \times u^{(1)}]\right\} - \frac{\nabla p^{(1)}}{\gamma} \qquad (1)$$

The total unsteady velocity vector can be broken up into acoustic, irrotational, and so-called vortical,[1] rotational parts

$$u_z^{(1)} = u_z' + \tilde{u}_z \quad \text{and} \quad u_r^{(1)} = u_r' + \tilde{u}_r \qquad (2)$$

where the acoustic part is obtained from the plane wave solution.[1] After splitting the velocities into rotational and irrotational components, the governing equation for the rotational velocity can be isolated:

$$\frac{\partial \tilde{u}}{\partial t} + M_b[\nabla(\tilde{u} \cdot U) - \tilde{u} \times (\nabla \times U) - U \times (\nabla \times \tilde{u})]$$

$$= \delta^2[\nabla \times (\nabla \times \tilde{u})] \qquad (3)$$

Since the time-dependent radial velocity has been shown to be negligible,[1,4–6,13–16] both analytically and numerically, the unsteady axial component of the equation will be the focus here.

Time-Dependent Viscous Boundary-Layer Equation

The present analysis then begins with the equation governing the axial rotational velocity derived first by Flandro,[13,14] where he used the assumption that the axial dependence is of the same order as the Mach number [Eq. (32) in Ref. 14]. Keeping the viscous term and using cylindrical coordinates, the axial component of Eq. (3) becomes

$$\frac{\partial \tilde{u}_z}{\partial t} + M_bU_r\frac{\partial \tilde{u}_z}{\partial r} = \delta^2\left(\frac{\partial^2 \tilde{u}_z}{\partial r^2} + \frac{1}{r}\frac{\partial \tilde{u}_z}{\partial r}\right) + \mathbb{O}(M_b) \qquad (4)$$

By retaining the viscous term in Eq. (4), the partial differential equation (PDE) is of second order, making it possible to satisfy both the sidewall no-slip condition and the centerline symmetry.

Using the forcing frequency time scale, time is rescaled so that Eq. (4) can be written in an alternative form

$$\frac{\partial \tilde{u}_z}{\partial \bar{t}} + \frac{M_b}{k}U_r\frac{\partial \tilde{u}_z}{\partial r} = \frac{\delta^2}{k}\left(\frac{\partial^2 \tilde{u}_z}{\partial r^2} + \frac{1}{r}\frac{\partial \tilde{u}_z}{\partial r}\right) \qquad (5)$$

where

$$\bar{t} = kt = (2\pi fR/a_0)t = 2\pi ft^* \qquad (6)$$

Equation (5) is linear; however, the convective term has a variable coefficient, U_r, which vanishes at the centerline. Closed-form analytical solutions to the previous equation appear to be possible only when Culick's[18] radial velocity component is approximated by a constant near the injection surface.[13,14] For $U_r = -1$, Flandro[14] derived a useful closed-form analytical solution that agrees very well near the surface with the numerical solution to the same equation using the exact radial velocity U_r. This solution is very helpful in analyzing the internal flowfield and, subsequently, the accompanying boundary-layer structure. Because of the approximation, this analytical solution is limited to a small range of physical parameters. As a rule of thumb, Flandro's[14] near-wall viscous solution will match the numerical solution to the same governing equation (with the exact Culick[18] velocity profile) as long as the penetration depth is less than about 45% of the chamber radius. For a larger boundary-layer thickness, the solution deteriorates rapidly. Descriptively, Flandro and Roach[1] and Flandro[14,15] state that this solution is valid only for sufficiently high frequencies or for low injection Mach numbers. As will be shown later, the limit of validity of Flandro's[14] solution will depend on a single parameter S_p, which will have to be smaller than 0.1 for the results to be accurate. This parameter, which controls the penetration depth of rotational waves, groups the dimensional blowing speed, circular frequency, kinematic viscosity, and chamber radius in the form

$$S_p = Re_a/St^3 = M_b^3/k^2\delta^2 = V_b^3/\omega^2\nu R \qquad (7)$$

It can be clearly seen that either a lower injection Mach number or a higher frequency can lead to a lower S_p. This coincides precisely with Flandro's[14] statement.

Improved Viscous Solution

Following Flandro's suggestion,[14] a closed-form perturbation solution that is applicable to a wider range of physical parameters can be obtained by using the exact Culick velocity profile U_r.[18] Since the highest derivative in Eq. (4) is multiplied by a small term δ^2, the methods of singular perturbation theory seem appropriate. It can be demonstrated that well-known perturbation techniques, with the exception of multiple scales, will fail to yield a uniformly valid solution in this case because the equation is singular at the centerline. In multiple scales, the

first step will be to find the correct local coordinate transformations that can be associated with the particular phenomena that dominate in a specific region of interest. In this problem, inertia and advection will dominate near the wall. Away from the wall, advection will become less significant since the radial velocity will become increasingly small.

Characteristic Scales

Since the solutions are periodic, time can be separated by introducing complex variables. By so doing, the parabolic PDE becomes a second-order ordinary differential equation (ODE) with complex variables. For $\tilde{u}_z(r, \bar{t}) = \bar{u}(r)\exp(i\bar{t})$, and

$$\varepsilon = \frac{\delta^2}{k} = \frac{1}{Re_a} = \frac{\nu}{2\pi fR^2} = \frac{\delta_s^2}{R^2} \approx \frac{\text{viscous forces}}{\text{unsteady inertia}}$$

$$\lambda = \frac{M_b}{k} = \frac{1}{St} = \frac{V_b}{2\pi fR} \approx \frac{\text{mean flow advection}}{\text{unsteady inertial forces}} \quad (8)$$

Equation (5) becomes the second-order governing ODE:

$$\underbrace{i\bar{u}}_{\text{Inertia}} + \underbrace{\lambda U_r \frac{d\bar{u}}{dr}}_{\text{Advection}} = \underbrace{\varepsilon \left(\frac{d^2\bar{u}}{dr^2} + \frac{1}{r} \frac{d\bar{u}}{dr} \right)}_{\text{Viscous Dissipation}} \quad (9)$$

External Scale

Near the wall, unsteady inertia and mean flow advection dominate when the speed of injection is larger than the speed of diffusion of shear waves. Viscous effects are still present, but their role is secondary. As a consequence of the injection, unsteady vorticity is generated at the wall. In an annulus near the wall of characteristic thickness $(1 - r)$, changes in the oscillating velocity are periodic, with almost constant amplitude. To obtain a balance between the dominant forces, a macroscopic spatial length scale must be used to account for these effects. Instead of stretching the spatial coordinate near the wall as done customarily in the inner region of steady boundary layers (where the velocity amplitude changes rapidly), a compression of the scale is required here since the oscillatory amplitude decays slowly near the wall where the effect of blowing is appreciable. In contracting the spatial dimension, a transformation of the independent variable is needed. Introducing the near-wall transformation variable $r_1 = \varepsilon(1 - r)$, a balance between unsteady inertia and advection is achieved from Eq. (9)

$$i\bar{u} - \varepsilon\lambda U_r \frac{d\bar{u}}{dr_1} = \varepsilon^3 \frac{d^2\bar{u}}{dr_1^2} - \frac{\varepsilon^2}{r_1} \frac{d\bar{u}}{dr_1} = \mathbb{O}(\varepsilon^2) \quad (10)$$

which explains the large observed velocity gradient of $\mathbb{O}(St)$ near the wall, since obtaining a balance between the first two terms in Eq. (10) requires that

$$\frac{d\bar{u}}{dr_1} = \mathbb{O}\left(\frac{1}{\varepsilon\lambda} \right) \quad \text{or} \quad \frac{d\bar{u}}{dr} = \mathbb{O}(\lambda^{-1}) \equiv \mathbb{O}(St) \quad (11)$$

Physically, this result can be translated into the fact that the steepness of propagating velocity waves will be dependent upon St.

Internal Scale

Moving away from the wall, unsteady inertia and viscous stresses will be in balance when radial advection becomes sufficiently weak. Blowing effects in this narrow region become secondary since the steady radial component of injection becomes small. The amplitude of the unsteady rotational velocity exhibits an exponential decay that will happen faster at higher viscosities. Viscous stresses exert forces that tend to damp out the amplitude of the oscillations. To obtain a balance between

viscous stresses and unsteady inertia, a microscopic spatial length scale must be carefully chosen. Since the rate of exponential decay of the unsteady rotational velocity amplitude increases toward the centerline, an expansion of the region is required to account for rapid spatial changes in amplitude. Instead of compressing the spatial coordinate as done near the wall, a stretching or magnification of the scale is required here. The inner edge of this region will correspond to the point where the rotational wave amplitude becomes vanishingly small. Beyond that point, the unsteady flow may be considered to be irrotational. Because of the injection at the wall, the traditionally thin and highly viscous region, which usually occurs at the wall in no-injection flowfields, is blown off the wall toward the centerline. Under such circumstances, the thin viscous layer becomes a free shear layer separating the highly rotational flow from the irrotational flow. This phenomenon is very similar to the Blowhard problem that was well described by Cole and Aroesty.[19] This region is also analogous to what is generally considered to be the thin inner region in steady boundary layers where the velocity profile changes in a relatively short distance to match the outer flowfield, which, in this case, will correspond to the inviscid and irrotational acoustic velocity component. In our problem, the penetration depth, which is defined as the distance from the wall to the inner edge of the viscous zone, will be a measure of the rotational field thickness. In stretching the radial coordinate in the inner region, a parameter transformation of the independent variable is sought. Introducing the centerline scale $r_1 = (r^n/\varepsilon)$, or its inverse (εr^{-n}), a balance between unsteady inertia and diffusion can be achieved. For $r_1 = (\varepsilon r^{-n})$, Eq. (9) becomes

$$i\bar{u} - n^2\varepsilon^{1-2/n} \left(r_1^{2(1+1/n)} \frac{d^2\bar{u}}{dr_1^2} + r_1^{(1+2/n)} \frac{d\bar{u}}{dr_1} \right)$$

$$= -n\varepsilon^{-1/n}r_1^{(1+1/n)}\lambda U_r \frac{d\bar{u}}{dr_1} = 0 \quad (12)$$

which shows that the inertial and viscous force terms will be of the same order of magnitude in this thin shear layer (where U_r vanishes) when $\varepsilon^{1-2/n} = 1$ or $n = 2$. Note that there is a transitional field between the inner and near-wall regions. When U_r is not negligible, a value of $n = 1$ in Eq. (12) will characterize this transitional zone.

Composite Scales

Nonunique composite scales that are valid in the entire region extending from the centerline to the wall can be constructed. By using $r_1 = \varepsilon(1 - r)/r^n$, with $1 \leq n \leq 2$ (n being a scale stretching coefficient), the compressed scale $\varepsilon(1 - r)$ near the wall will result (in the vicinity of $r = 1$), and the magnified scale ε/r^n will result as the centerline is approached. This composite scale leads to a closed-form expression that agrees with the numerical solution in the entire range of the independent variable with a margin of uncertainty that is smaller than that associated with the mathematical model itself.

Perturbation Methods

Equation (9), that we propose to solve using perturbation techniques, contains a turning point at the centerline (where the advection term vanishes), and a region of nonuniformity in its vicinity. The boundary conditions can be translated as

$$\begin{cases} \bar{u}(r = 1) = -1 & \text{(no slip condition)} \\ \dfrac{d\bar{u}}{dr} (r = 0) = 0 & \text{(symmetry condition)} \end{cases} \quad (13)$$

The solution type is oscillatory with decaying amplitudes, exhibiting large localized velocity gradients at the extrema. Since Eq. (9) is singular, no single asymptotic expansion will be uniformly valid throughout the entire field of interest.[20] The

classical techniques of regular perturbation become invalid for such a singular problem. Methods of strained coordinates are not capable of yielding uniformly valid expansions either, in cases in which sharp changes in the dependent variable (velocity) take place in some domain of the independent variable.[21] To obtain uniformly valid expansions, it must be recognized that the sharp changes are characterized by modified scales that are different from the scales characterizing the behavior of the dependent variable outside the sharp-change region. The solution will have to be sought separately in the different regions of the domain, and a composite solution will have to be constructed such as to match the individual solutions in their respective fields. For singular problems with a region of nonuniformity, coincidentally referred to as a boundary-layer region, a matched asymptotic expansion procedure is generally used to relate the expansions in the scale-dependent regions. Unfortunately, the matched asymptotic expansion procedure cannot be used on Eq. (9), since it violates the conditions of existence of a unique solution. Using mathematical conditions stated by Nayfeh,[21] for a second-order ODE with the smallest term ε multiplying the highest derivative, a matched asymptotic procedure will be successful for this problem if one of the conditions given next is met

$$-\lambda U_r = (1/St)[\sin(\theta)/r] > 0 \quad \text{at} \quad r = 0 \quad \text{(centerline)} \quad (14)$$

$$-\lambda U_r = (1/St)[\sin(\theta)/r] < 0 \quad \text{at} \quad r = 1 \quad \text{(wall)} \quad (15)$$

It is clear that neither condition is satisfied here. The method of multiple scales appears to be the major technique remaining.

The solution can be written using a two-term perturbation:

$$\bar{u}(r_0, r_1) = \bar{u}_0(r_0, r_1) + \varepsilon \bar{u}_1(r_0, r_1) + \mathbb{O}(\varepsilon^2) \quad (16)$$

The two scales are the base $r_0 \equiv r$ and the modified scale $r_1 \equiv \varepsilon s(r) \equiv \varepsilon s(r_0)$, where $s(r)$ is the scale function

$$s(r) = \begin{cases} 1 - r, & \text{near the wall} \\ r^{-n}, & \text{in the free shear layer} \\ (1 - r)r^{-n}, & \text{composite scale} \end{cases} \quad (17)$$

Using the chain rule for differentiation, transforming Eq. (9) from a function of a single variable r into a PDE dependent on the two scales r_0 and r_1, substituting Eq. (16), the perturbed two-term approximation for $\bar{u}$ into the resulting PDE, rearranging and collecting terms of order ε^0 and ε^1, two first-order coupled PDEs result

$$i\bar{u}_0 + \lambda U_r \frac{\partial \bar{u}_0}{\partial r_0} = 0 \quad (18)$$

or

$$\bar{u}_0(r_0, r_1) = C_0(r_1)\exp((i/\pi\lambda)\ell n\{\tan[(\pi/4)r_0^2]\}) \quad (19)$$

$$i\bar{u}_1 + \lambda U_r \frac{\partial \bar{u}_1}{\partial r_0} = -\lambda U_r \frac{ds}{dr_0}\frac{\partial \bar{u}_0}{\partial r_1} + \frac{\partial^2 \bar{u}_0}{\partial r_0^2} + \frac{1}{r_0}\frac{\partial \bar{u}_0}{\partial r_0} \quad (20)$$

After substituting Eq. (19), the integrated value of $\bar{u}_0$ from Eq. (18) into Eq. (20), the right-hand side (RHS) of Eq. (20) becomes a source of secular terms. To avoid secular terms that cause the solution to break down, a mathematical requirement that satisfies the centerline symmetry condition is that the RHS of Eq. (20) be zero. This condition, in addition to the no-slip constraint at the wall ($\bar{u} = -1$), allows the determination of $C_0(r_1)$, and hence, the first term of the multiple-scales solution. The unsteady axial velocity including acoustic–irrotational and vortical–rotational components can now be constructed for any scale function $s(r)$.

Letting

$$\eta(r) = s(r) \left(\frac{ds}{dr}\right)^{-1} \quad (21)$$

$$u_z^{(1)} = [\sin \bar{t} - e^{\xi} \sin(\bar{t} + \Phi)]\sin(kz) \quad (22)$$

with

$$\xi = (St^3/Re_a)[r^3\eta(r)\csc^3\theta - \eta(1)] \quad (23)$$

$$\Phi(r) = \Phi_0(r) + \Phi_1(r) \quad (24)$$

where the inviscid and viscous terms are

$$\Phi_0 = (St/\pi)\ell n \tan(\theta/2) \quad (24a)$$

$$\Phi_1 = -(St^2/Re_a)[r \csc^2\theta(2 - \pi r^2 \cot \theta)\eta - 2\eta(1)] \quad (24b)$$

Here, $\Phi(r)$ determines the propagation speed of the shear wave, being the phase angle of the rotational axial velocity component with respect to the acoustic counterpart at a fixed value of r. On the other hand, $\xi(r)$, representing the rate of viscous damping, controls the thickness of the outer wave envelope. Hence, it controls the thickness of the boundary layer. The penetration depth, defined by determining the radial position at which the rotational wave amplitude decays to 1% of the acoustical amplitude, will only depend on one parameter Re_a/St^3, or the penetration number S_p. When measured from the solid wall, the penetration depth can be found from $y_p = 1 - r_p$, where r_p is the root to

$$r_p^3\eta(r_p)\csc^3(\pi r_p^2/2) - \eta(1) + S_p \ell n(100) = 0 \quad (25)$$

Practical Rocket Range of Physical Parameters

In combustion instability, variations exist in physical parameters and sizing, ranging from cold-flow experiments with low kinematic viscosity to rockets with high temperatures and pressures. Based on cases exhibiting intermediate to low-frequency instability, Table 1 is adapted from Ref. 22 to define the range (min, max) of key parameters.

Unsteady Axial Velocity and Penetration Depth

For the unsteady axial velocity, the solution assumes $u_z^{(1)}$ in the form[1,14] of Eq. (22) given earlier.

Simplified Version of Flandro's Analytic Solution

Flandro's solution[14] is restated here to point out its usefulness and reformulate it in a more compact form that is a result of expressing it in terms of S_p. The simplification takes advantage of the fact that Re_a, being the square of the ratio of the tube radius to the Stokes-layer thickness, is a large number, exceeding 10^4 in practice:

$$\xi = S_p^{1/3}Re_a^{2/3}[1 - \sqrt{0.5(1 + C)}](y/2) \cong -(y/S_p) \quad (26)$$

$$\Phi = -S_p^{1/3}Re_a^{2/3}\sqrt{0.5(-1 + C)}(y/2) \cong -Sty \quad (27)$$

$$C = (1 + 16S_p^{-4/3}Re_a^{-2/3})^{1/2} \cong 1 + 8S_p^{-4/3}Re_a^{-2/3} \quad (28)$$

from which the boundary-layer thickness can be derived

$$y_p = \frac{2 \ell n(100)S_p^{-1/3}Re_a^{-2/3}}{-1 + \sqrt{0.5(1 + C)}} \cong Y \quad (29)$$

This solution is valid when $S_p \leq 0.1$, corresponding to a penetration depth that does not exceed $0.46R$. Equation (22), when simplified, can be used to retrieve valuable information about

Table 1 Practical range of control parameters

f, Hz	R, m	ν	V_b	Re_a	St	S_p
10.00	0.025	5^{-6}	2	10^4	10.00	0.02
1500	3.000	2^{-4}	7	10^8	1700	300

the unsteady velocity amplitude, wavelength, and phase lag with respect to pressure:

$$u_z^{(1)} = [\sin(kt) - e^{-y/S_p} \sin(kt - Sty)]\sin(kz) \qquad (30)$$

Equation (30) shows that S_p controls the thickness and St, the wavelength of $u_z^{(1)}$. Both control the phase of the velocity relative to the acoustic pressure.

Near-Wall Solution

$$s(r) = 1 - r, \qquad \eta = -(1 - r), \qquad \xi = -S_p^{-1}r^3(1 - r)\csc^3\theta \qquad (31)$$

$$\Phi_1(r) = (St^2/Re_a)[r(1 - r)\csc^2\theta(2 - \pi r^2 \cot\theta)] \qquad (32)$$

To obtain y_p, one solves: $(1 - r_p)r_p^3 + Y \sin^3(\pi/2)r_p^2 \equiv 0$, knowing that y_p possesses an asymptotic solution, for small S_p, which approaches Flandro's near-wall result[14]

$$y_p \cong Y(1 + Y + 4Y^2)^3 \cong Y(1 + 3Y) \qquad (33)$$

For practical purposes, the near-wall perturbed and Flandro's linearized solutions[14] match very well.

Inner Solution

$$s(r) = r^{-2}, \qquad \eta = -(r/2), \qquad \xi = -S_p^{-1}[(r^4 \csc^3\theta - 1)/2] \qquad (34)$$

$$\Phi_1(r) = (St^2/2Re_a)[r^2 \csc^2\theta(2 - \pi r^2 \cot\theta) - 2] \qquad (35)$$

Yielding $r_p^4 - (1 + 2Y) \sin^3(\pi/2)r_p^2 \equiv 0$, with a very accurate asymptotic solution, near the centerline

$$r_p \cong \sqrt[4]{\frac{32}{3\pi^2}} \sin^{1/2}\left\{-\frac{\pi}{6} + \frac{\arccos}{3}\left[\frac{-6\sqrt{3/2}}{\pi^2(1 + 2Y)}\right]\right\} \qquad (36)$$

Composite Solution

$$s(r) = (1 - r)r^{-n}, \qquad \eta = \frac{(1 - r)r}{r(n - 1) - n} \qquad (37)$$

where

$$1 \le n \le 2, \qquad \xi = -S_p^{-1}\frac{(1 - r)r^4}{n - r(n - 1)}\csc^3\theta$$

$$\Phi_1(r) = \frac{St^2}{Re_a}\frac{r^2(1 - r)}{n - r(n - 1)}\csc^2\theta(2 - \pi r^2 \cot\theta) \qquad (38)$$

with a penetration depth that can be computed from

$$r_p^4(1 - r_p) + Y[r_p(n - 1) - n]\sin^3(\pi/2)r_p^2 \equiv 0 \qquad (39)$$

to which an expansion of $\mathbb{O}(r_p^6)$ can be derived; $n > 1$:

$$r_p \cong \frac{e}{3} - 2g \sin\left[\frac{\pi}{6} - \frac{\arccos}{3}\left(\frac{h}{2g^3}\right)\right] \qquad (40)$$

where

$$e = \frac{n}{n - 1}, \qquad f = \frac{8}{3\pi^3(n - 1)Y}, \qquad g = \sqrt{f + \frac{e^2}{9}}$$

$$h = \frac{2}{27}e^3 - f\frac{2n - 3}{n - 1}$$

which, for $n = 1$, a particular case arises having an expansion

$$r_p \cong (4/\pi^3 Y)(\sqrt{1 + \pi^3 Y/2} - 1) \qquad (41)$$

Flandro's New Inviscid Solution

Recently, Flandro[15] derived an inviscid solution that includes the axial convection of vorticity. Accordingly, the damping of the rotational velocity wave amplitude is attributed to the weakening of unsteady vorticity resulting from the axial, downstream convection caused by the steady flow motion toward the chamber exit cone. This solution has the advantage of including the axial dependence. Its limitation is that it is inviscid.

Phase Angle Relative to Pressure

At the wall, Φ has an exact analytical limit that is common to all solutions in Eqs. (27), (32), (35), and (38). The unsteady velocity-to-pressure phase angle can be derived (see Fig. 1) as $\beta = \text{Arctan}(StS_p) - 90$ deg. This result, of a small phase at the wall, agrees with conclusions drawn from numerical so-
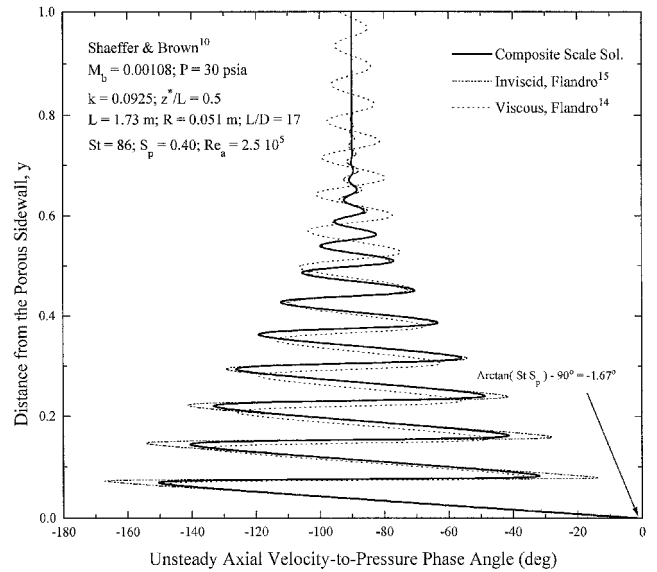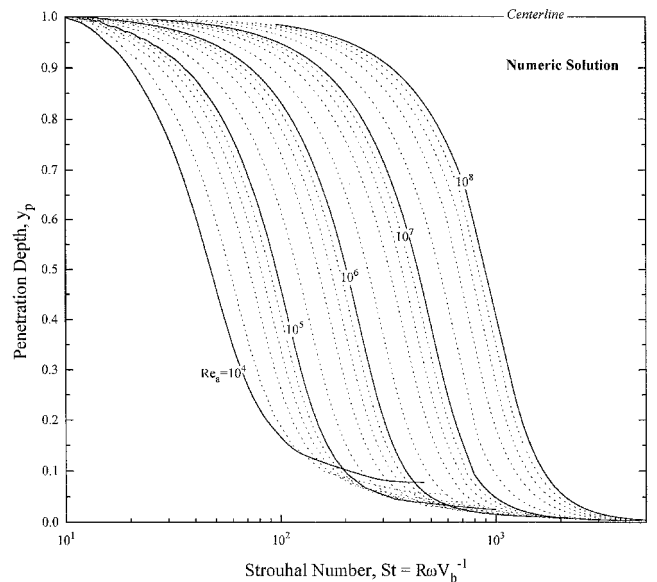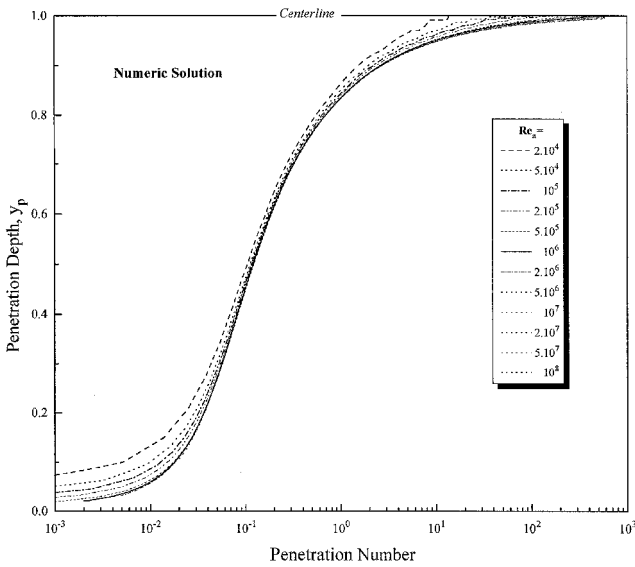
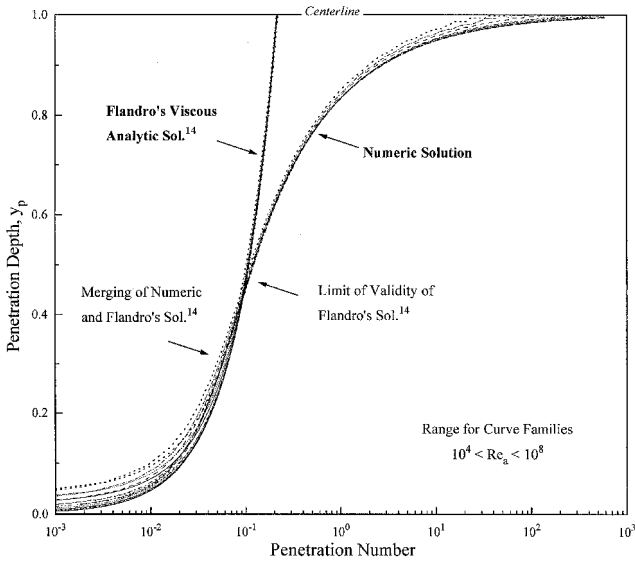**Fig. 1   Unsteady velocity-to-pressure phase lag.**
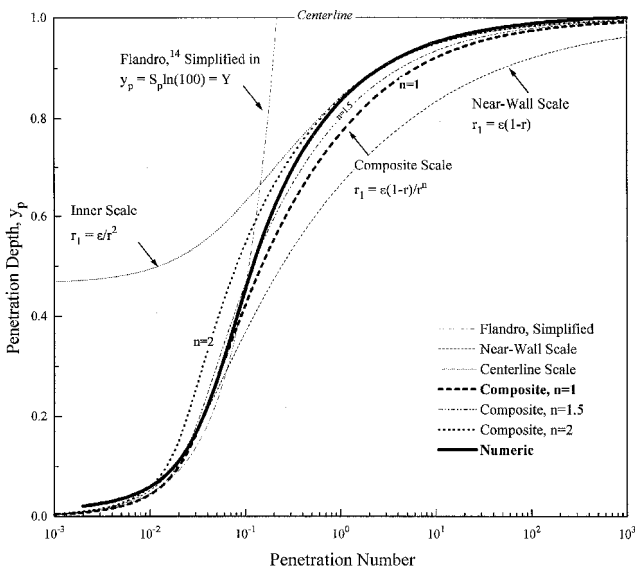
Fig. 2   Penetration depth function of St and Re_a

Fig. 3   Penetration depth as function of S_p.

Fig. 4   Flandro's penetration depth[14] as function of S_p.

Fig. 5   Comparison of analytic and numeric y_p.

lutions.[1,5,6] Near the centerline where the acoustic velocity is the only nonzero component, β will be -90 deg.

Numerical Solution

Equation (4) can be solved numerically. Being a highly stiff equation, superposition will be required in addition to a shooting procedure that starts at the wall, and integrates back to the centerline. A family of curves can be generated that depends on two controlling dynamic parameters, St and Re_a. This family of curves collapses into a single line (see Figs. 2 and 3) when S_p is used as the independent variable. This dependence on S_p becomes even stronger at higher Re_a (when $\varepsilon \to 0$).

Analytic and Numeric Penetration Depth Solutions

Figure 4 shows clearly that Flandro's viscous solution[14] matches the numeric solution in the bottom half of the domain. Figure 5 shows the validity of multiple-scales solutions in their regions of applicability. Note the accuracy of the internal and
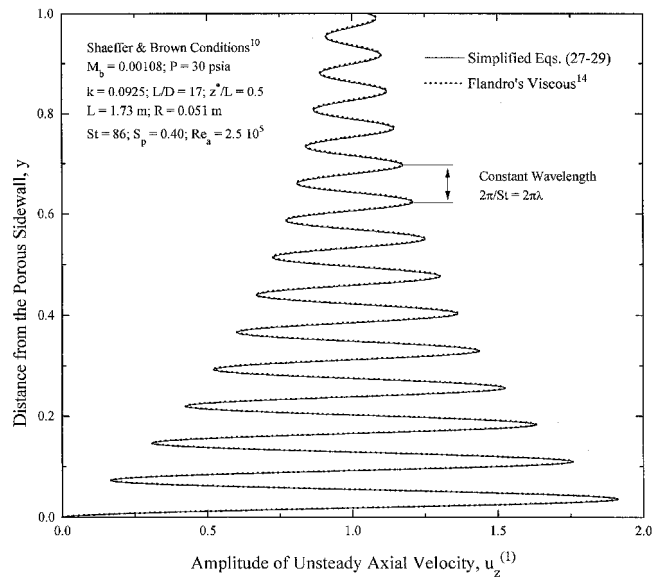
Fig. 6   Simplified version of Flandro's solution.[14]
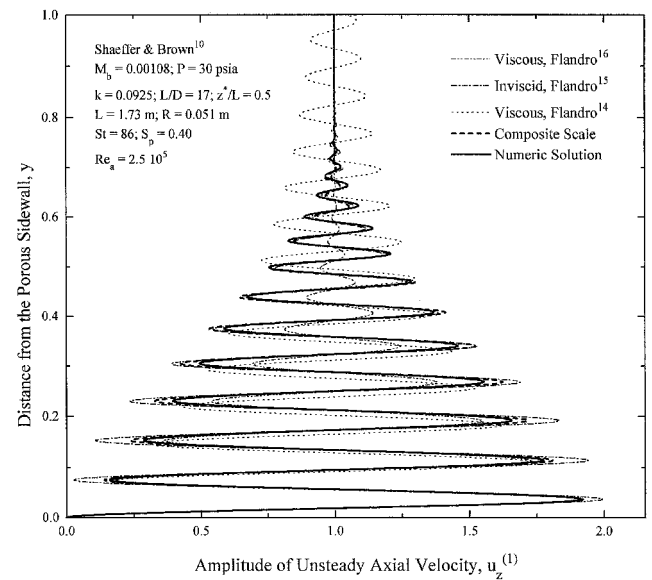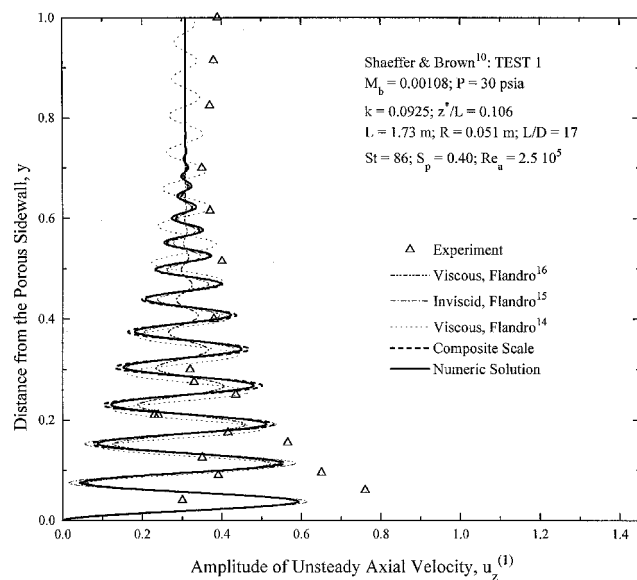

Fig. 7   Typical solutions at $z^*/L = 0.5$.

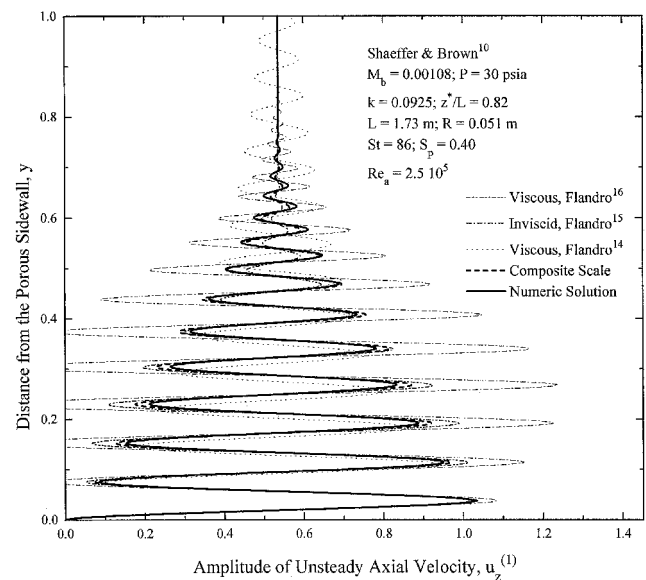**Fig. 8   Comparison to experimental data at $z^*/L = 0.1$.**

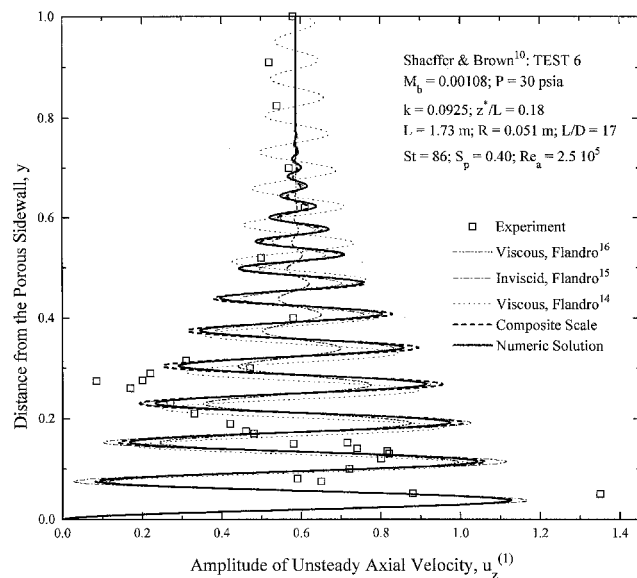**Fig. 10   Comparison of solutions at $z^*/L = 0.82$.**

Fig. 9   Comparison to experimental data at $z^*/L = 0.2$.

external scales in extracting the solution in the upper and lower quarter domains, respectively. Also, note the usefulness of the composite scale solution in the upper half of the domain where Flandro's[14] approximate solution deteriorates.

Unsteady Velocity Profiles

Figure 6 shows that the agreement between Flandro's viscous solution[14] and the simplified solution (30) is dramatic. Figure 7 shows a fair agreement between existing models at the axial midpoint. Figures 8 and 9 show a good agreement with experimental data near the chamber fore-end. In every case, the depth of the rotational region is slightly overpredicted by models that do not incorporate either the axial convection of unsteady vorticity by the mean flow or the viscous effects. Figure 10 shows a disagreement between existing models and Flandro's inviscid solution[15] when approaching the aft end of the chamber. It appears that both the axial dependence and viscous effects are important to achieve an accurate description of the boundary-layer structure.

Conclusions

The classical concepts of boundary-layer theory regarding inner, near-wall and outer, external regions are not applicable for the case of an oscillating flow over a transpiring surface. Near the wall, a thick highly rotational layer is established near the solid boundary when hard blowing persists because of vorticity production and convection. The thin layer where viscous friction is important is blown off the wall to form a free shear layer (that cannot be localized), separating rotational and irrotational flowfields. The penetration depth, or acoustic boundary-layer thickness, is a measure of the region where rotational effects are important. It is function of a similarity parameter that is proportional to the cube of the injection speed, inversely proportional to the square of the frequency, and inversely proportional to the viscosity and chamber effective radius. This dependence is in total agreement with empirical observations as well as numerical analyses. Accordingly, the role of viscosity is to attenuate the amplitude of propagating shear waves and to shorten, rather than extend, the penetration depth. The role of intrinsic or imposed frequency of oscillations is similar to viscosity, only more important. Quadrupling the viscosity requires half the frequency for the same profile thickness when all other parameters are held constant. Higher acoustic modes (and therefore oscillation frequencies) in the chamber will lead, naturally, to smaller penetration depths. The role of the Strouhal number as the controlling parameter for the vortical-to-acoustical phase angle has again been demonstrated. The scaling analysis clearly shows that increasing the Strouhal number will steepen the rotational wave crest and reduce its spatial wavelength. Pertinent to this type of asymptotic expansion problems, the method of multiple scales appears to be a powerful tool in extracting analytic solutions. It appears that neglecting the axial dependence is a good approximation only near the chamber head-end. Inclusion of the axial convection of vorticity is needed for a more accurate solution. Finally, the phenomena of importance in the rotational time-dependent momentum equation have been identified to be 1) unsteady inertia, 2) radial convection of unsteady vorticity by Culick's radial velocity component, 3) viscous diffusion of vorticity, and 4) axial convection of vorticity caused by downstream convection by Culick's axial velocity component. Since the present analysis did not include the latter term, it is hoped that a more complete solution based on the perturbation approach outlined here can be achieved including the axial dependence.

Acknowledgment

References

[1]Flandro, G. A., and Roach, R. L., "Effects of Vorticity Production on Acoustic Waves in a Solid Propellant Rocket," Final Rept., Air Force Office of Scientific Research, Contract 90-0159, 1992.

[2]Beddini, R. A., and Roberts, T. A., "Turbularization of an Acoustic Boundary-Layer on a Transpiring Surface," AIAA Paper 86-1448, June 1986.

[3]Beddini, R. A., and Roberts, T. A., "Response of Propellant Combustion to a Turbulent Acoustic Boundary Layer," AIAA Paper 88-2942, July 1988.

[4]Smith, T. M., Roach, R. L., and Flandro, G. A., "Numerical Study of the Unsteady Flow in a Simulated Rocket Motor," AIAA Paper 93-0112, Jan. 1993.

[5]Vuillot, F., and Avalon, G., "Acoustic Boundary Layer in Large Solid Propellant Rocket Motors Using Navier-Stokes Equations," *Journal of Propulsion and Power*, Vol. 7, No. 2, 1991, pp. 231–239.

[6]Vuillot, F., "Numerical Computation of Acoustic Boundary Layers in Large Solid Propellant Space Booster," AIAA Paper 91-0206, Jan. 1991.

[7]Sabnis, J. S., Giebeling, H. J., and McDonald, H., "Navier-Stokes Analysis of Solid Propellant Rocket Motor Internal Flows," *Journal of Propulsion and Power*, Vol. 5, No. 6, 1989, pp. 657–664.

[8]Baum, J. D., "Numerical Study of Flow Turning Phenomenon," AIAA Paper 86-0533, Jan. 1986.

[9]Culick, F. E. C., and Yang, V., "Stability Predictions in Rockets," *Nonsteady Burning and Combustion Stability of Solid Propellants*, Vol. 143, Progress in Astronautics and Aeronautics, AIAA, Washington, DC, 1992, pp. 719–799.

[10]Shaeffer, C. W., and Brown, R. S., "Oscillatory Internal Flow Studies," United Technologies, Chemical Systems Div., Rept. 2060 FR, Sunnyvale, CA, Aug. 1992.

[11]Zhao, Q., and Kassoy, D. R., "The Generation and Evolution of Unsteady Vorticity in a Model of a Solid Rocket Engine Chamber," AIAA Paper 94-0779, Jan. 1994.

[12]Kirkkopru, K., Kassoy, D. R., and Zhao, Q., "Unsteady Vorticity Generation and Evolution in a Model of a Solid Rocket Motor: Sidewall Mass Addition Transients," AIAA Paper 95-0603, Jan. 1995.

[13]Flandro, G. A., "Solid Propellant Acoustic Admittance Corrections," *Journal of Sound and Vibration*, Vol. 36, No. 3, 1974, pp. 297–312.

[14]Flandro, G. A., "Effects of Vorticity Transport on Axial Acoustic Waves in a Solid Propellant Rocket Chamber," American Society of Mechanical Engineers Annual Meeting, San Francisco, CA, Dec. 1989.

[15]Flandro, G. A., "Effects of Vorticity on Rocket Combustion Stability," *Journal of Propulsion and Power*, Vol. 1, No. 4, 1995, pp. 607–625.

[16]Flandro, G. A., "On Flow Turning," AIAA Paper 95-2730, July 1995.

[17]Richardson, E. G., and Tyler, E., *Proceedings of the Physical Society of London*, Vol. 42, 1929, p. 1.

[18]Culick, F. E. C., "Rotational Axisymmetric Mean Flow and Damping of Acoustic Waves in a Solid Propellant Rocket," *Journal of Propulsion and Power*, Vol. 5, No. 6, 1989, pp. 657–664.

[19]Cole, J. D., and Aroesty, J., "The Blowhard Problem-Inviscid Flows with Surface Injection," *International Journal of Heat and Mass Transfer*, Vol. 11, July 1968, pp. 1167–1183.

[20]Van Dyke, M., *Perturbation Methods in Fluid Mechanics*, The Parabolic Press, Stanford, CA, 1975.

[21]Nayfeh, A., *Perturbation Methods*, Wiley, New York, 1973.

[22]Nickerson, G. R., Coates, D. E., and Hermsen R. W., "A Computer Program for the Prediction of Solid Propellant Rocket Motor Performance," Air Force Rocket Propulsion Lab., Interim Technical Rept. 80-34, April 1981.